

pubs.acs.org/JPCB Article

Local Hydrogen Bonding Determines Branching Pathways in Intermolecular Heptazine Photochemistry

Published as part of The Journal of Physical Chemistry virtual special issue "Early-Career and Emerging Researchers in Physical Chemistry Volume 2".

Doyk Hwang,[#] Liam M. Wrigley,[#] Micah Lee, Andrzej L. Sobolewski, Wolfgang Domcke, and Cody W. Schlenker*



Cite This: J. Phys. Chem. B 2023, 127, 6703-6713



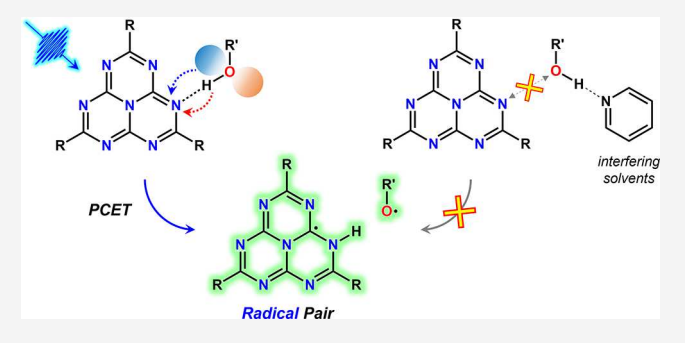
ACCESS I

III Metrics & More

Article Recommendations

Supporting Information

ABSTRACT: Heptazine is the molecular core of the widely studied photocatalyst carbon nitride. By analyzing the excited-state intermolecular proton-coupled electron-transfer (PCET) reaction between a heptazine derivative and a hydrogen-atom donor substrate, we are able to spectroscopically identify the resultant heptazinyl reactive radical species on a picosecond time scale. We provide detailed spectroscopic characterization of the tri-anisole heptazine:4-methoxyphenol hydrogen-bonded intermolecular complex (TAHz:MeOPhOH), using femtosecond transient absorption spectroscopy and global analysis, to reveal distinct product absorption signatures at ~520, 1250, and 1600 nm. We assign these product peaks to the hydrogenated TAHz radical (TAHzH•)



based on control experiments utilizing 1,4-dimethoxybenzene (DMB), which initiates electron transfer without concomitant proton transfer, *i.e.*, no excited-state PCET. Additional control experiments with radical quenchers, protonation agents, and UV—vis—NIR spectroelectrochemistry also corroborate our product peak assignments. These spectral assignments allowed us to monitor the influence of the local hydrogen-bonding environment on the resulting evolution of photochemical products from excited-state PCET of heptazines. We observe that the preassociation of heptazine with the substrate in solution is extremely sensitive to the hydrogen-bond-accepting character of the solvent. This sensitivity directly influences which product signatures we detect with time-resolved spectroscopy. The spectral signature of the TAHzH• radical assigned in this work will facilitate future in-depth analysis of heptazine and carbon nitride photochemistry. Our results may also be utilized for designing improved PCET-based photochemical systems that will require precise control over local molecular environments. Examples include applications such as preparative synthesis involving organic photoredox catalysis, on-site solar water purification, as well as photocatalytic water splitting and artificial photosynthesis.

■ INTRODUCTION

Proton-coupled electron transfer (PCET) is important in numerous energy conversion processes, ranging from photosynthesis to recent developments in catalysis and fuel cell operation. The coupled motion of an electron and proton can lower the energy barrier of a reactive pathway by avoiding high-energy intermediates, facilitating important processes to catalyze synthetic reactions, transfer drive photocatalytic water splitting, and generate solar fuels. Of particular interest are PCET processes in hydrogen-bonded molecular complexes. The importance of preassociative hydrogen bonding for PCET has been explored in many organic and organometallic systems where O–H and N–H groups in the substrate can be activated for further chemical reactions. Also, it is widely understood that hydrogen-bond networks appear to be critical in PCET processes of biological systems

such as photosystem II.^{22–24} These studies indicate that relatively small changes in the hydrogen-bonding environment may substantially influence the preassociation steps of molecular complexes and the outcome of the PCET reaction.^{25–29} The influence of hydrogen bonding is particularly important for photoinduced PCET of intermolecular complexes, where the hydrogen bonding not only significantly facilitates the intermolecular PCET process through preassociation^{12,28} but also improves chemoselectivity

Received: February 28, 2023 Revised: June 29, 2023 Published: July 20, 2023





of certain photoreactions,^{30,31} which otherwise have to occur through rather slow, randomly oriented diffusional collisions within the solvent.

While PCET processes are widely recognized to be critical in molecular photochemistry, reports considering the importance of such processes for designing materials for solar photocatalysis are less abundant. One notable example is the case of carbon nitride, a polymeric photoactive material comprising monomeric heptazine (Hz) units. Although carbon nitride has been extensively studied, 32-37 due to its facile synthesis and photocatalytic activity toward various chemical reactions, the preponderance of carbon nitride literature focuses on proton reduction reactions in the presence of excess sacrificial electron donors. However, when these sacrificial agents are removed, it has been shown that carbon nitride can drive full water splitting via a two-electron water oxidation route.³⁸ While photoinduced PCET may ultimately be shown to play a critical role in the initial stages of this water oxidation process, the fundamental aspects of the PCET processes that Hz derivatives can support have received less attention in the literature. However, Domcke, Sobolewski, and co-workers suggested, based on results from ab initio calculations, that intermolecular complexes formed by hydrogen bonding between the Hz moiety and water can help facilitate water oxidation. Within that theoretical framework, photoexcitation of this intermolecular complex triggers a PCET reaction that oxidizes water molecules to radical-pair products. Computational results of Domcke, Sobolewski, and co-workers, 39-41 as well as others, 42-44 have suggested that this initial oxidation step may comprise a reaction pathway for carbon nitride photocatalysts to drive water splitting. However, there have been a limited number of systematic experimental analyses to investigate this photoinduced PCET pathway between Hz moieties and protic substrates. The scarcity of these studies may be due, in part, to the inherent structural complexity of polymeric carbon nitrides, which can obscure mechanistic

Our group has spectroscopically explored the photoinduced PCET scenario with a stable, well-defined model molecular Hz derivative, tri-anisole-heptazine (TAHz). Our prior work revealed that TAHz can form hydrogen-bonded intermolecular complexes with H-atom donor substrates, such as water or various phenol derivatives, and undergoes intermolecular PCET from the substrate to TAHz upon near-UV photoexcitation. 47 In this process, the hydrogen atom is transferred from the substrate to TAHz through PCET, generating radicalpair products. With parasubstituted phenol derivatives of different oxidation potentials, we were able to control the PCET reactivity of TAHz by changing the energy barrier and observing barrierless excited-state reactivity for 4-methoxyphenol (MeOPhOH).⁴⁹ Additionally, we demonstrated that we could utilize sequential near-UV and NIR laser pulses to excite the TAHz:R-PhOH hydrogen-bonded intermolecular complex and optically control the PCET reaction.⁵⁰ More recently, we systematically varied the hydrogen-bonding nature between the phenolic substrate and TAHz. We investigated the effect of hydrogen bonding on TAHz photochemistry using timeresolved photoluminescence (TR-PL) measurements, combined with density functional theory (DFT) calculations. 51 We observed that stronger hydrogen bonding suppressed the change of molecular geometry of TAHz between the ground and the excited state and facilitated the PCET reactivity of the TAHz:R-PhOH complex.

One shortcoming in our prior work was that we were previously unable to experimentally resolve how radical product formation was directly influenced by the local hydrogen-bonding environment of the TAHz:substrate complex. In other words, we were previously only able to detect the disappearance of reactants and not the appearance of products. This void in our analysis left a deficiency for understanding the underlying reactivity mechanism. In this paper, we spectroscopically analyze how hydrogen-bond preassociation facilitates photoinduced radical-pair formation, using TAHz and MeOPhOH as a model testbed for understanding how intermolecular PCET from protic substrates occurs for carbon nitride-based photocatalysts. We identified spectroscopic signatures of the hydrogenated TAHz radical product (TAHzH•) using time-resolved pump-probe spectroscopy and global analysis. We find that three new peaks that appear when TAHz is exposed to MeOPhOH under near-UV illumination are attributable to TAHzH absorption. Identifying the TAHzH spectral signature allowed us to analyze the TAHz photochemistry based on the behavior of the photogenerated products, as opposed to simply evaluating the disappearance of photoreactants as we had in our prior studies. These new results provide a more precise handle to understand the PCET photochemistry of Hz derivatives. Additionally, employing solvents with varying competitive hydrogenbonding activity, we observed a modulation of the intermolecular hydrogen-bonding interactions between TAHz and MeOPhOH. Thereby, we were able to directly probe the influence of hydrogen bonding on intermolecular PCET and radical-pair product generation. Results from this study will help establish a detailed mechanistic picture of the reactivity of carbon nitride photocatalysts, with TAHz serving as a molecular model for the photooxidative activity of its polymeric heptazine counterparts. Furthermore, we anticipate that this study will be applicable to other PCET-based energy conversion systems where inter- and intramolecular hydrogen bonding plays an important role, such as photocatalytic synthesis⁷ and solar fuel generation.

MATERIALS AND METHODS

Synthesis. We synthesized TAHz according to our previous reports⁴⁷ from cyameluric chloride via a Friedel–Crafts reaction with anisole.

Sample Preparation. TAHz was dissolved at 100 μ M in toluene and diluted to target concentration for measurements (15 μ M for ground-state absorption, 50 μ M for time-resolved spectroscopy). TAHz solutions were sonicated for 5 min before measurements to ensure minimal aggregation effects. Samples were kept in the dark until measurements were performed. Phenol (Sigma-Aldrich), p-cresol (TCI), 4-methoxyphenol (TCI), 1,4-dimethoxybenzene (TCI), toluene (Fisher), anisole (Sigma-Aldrich), benzonitrile (TCI), and pyridine (Fisher) were used as received without further purifications. The 4-tert-butylcatechol stabilizer in styrene (TCI) was removed by washing twice with 10% sodium hydroxide and three times with distilled water, followed by drying with silica gel.

Ground-State Absorption and TAHz:MeOPhOH Hydrogen-Bonding Characterization. Ground-state absorption spectra were collected using a Cary 5000 UV-vis-NIR spectrometer. For the data collected in Figures 3 and S8, the initial TAHz concentration was 15 μ M in the chosen solvent and volume of the solution was 3 mL. Using a 3 M MeOPhOH

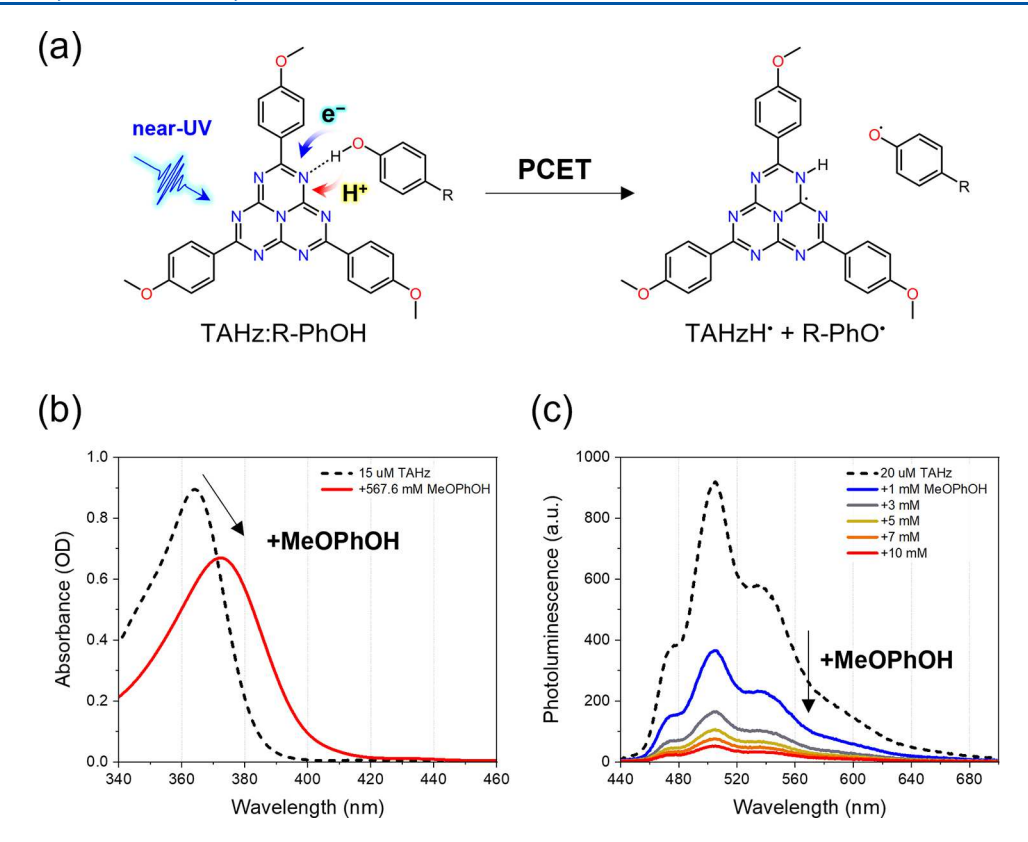


Figure 1. (a) Molecular structure of TAHz in a hydrogen-bonded complex with a phenol derivative. Upon excitation with 365 nm light, TAHz in its excited state undergoes an intermolecular excited-state proton-coupled electron transfer (PCET), forming a biradical species of a heptazinyl radical and a phenoxy radical. (b) Normalized absorption spectrum of TAHz in toluene (15 uM, black dash) compared with the spectrum of TAHz + MeOPhOH in toluene (+567.6 mM MeOPhOH, red). Hydrogen bonding leads to a red shift of transition to the bright $\pi\pi^*$ state at 365 nm. (c) Photoluminescence (PL) quenching of TAHz (20 uM) with increasing concentration of MeOPhOH, due to hydrogen bonding and excited-state PCET reaction.

stock, 20 μ L aliquots of the MeOPhOH stock were added to the TAHz solution and stirred, and an UV-vis absorption spectrum was recorded. This process was replicated to produce 10 sequential dilutions. Then, 50 μ L aliquots were added, stirred, and an UV-vis absorption spectrum was recorded 10 times. The resulting 21 spectra (one without MeOPhOH and 20 with sequential MeOPhOH additions) were baseline-corrected by subtracting background. The background for each spectrum was obtained from the average OD in the wavelength range of 495–500 nm of an UV-vis absorption spectrum with a blank sample, which contains the solvent and an equivalent addition of MeOPhOH. The ratio of concentration of MeOPhOH and TAHz was calculated by accounting for the change in volume upon each addition. Experimental details are shown in the Supporting Information (Section S1).

Spectroelectrochemistry. Spectroelectrochemistry was performed with TAHz (400 μ M) in an air-free tetrahydrofuran (THF) solution with tetrabutylammonium hexafluorophosphate (TBAPF₆) electrolyte (250 mM). A platinum mesh electrode was used as the working electrode, submerged in an air-free quartz cuvette with 1 cm path length. A platinum wire was used as a counter electrode, and a clean silver wire served as a pseudoreference. The electrochemical cell was held at set potentials using a Metrohm Autolab PGSTAT204 with NOVA Software v.2.1.4 and the change in the absorption spectra was collected over time using fiber-coupled Avantes AvaSpec-2048-USB2 (StarLine) and Avantes AvaSpec-NIR256-1.7-EVO spectrometers.

Transient Absorption Spectroscopy. The transient absorption (TA) spectroscopy setup is based on the Helios spectrometer from Ultrafast Systems. Samples were irradiated with the 365 nm ($\sim 1.4 \times 10^{15}$ photons/cm²/pulse or ~ 1 mW) output of an OPA (Coherent, Inc./Light Conversion OPerA Solo) that was pumped with 50 fs pulses from a 1 kHz, 800 nm Ti:sapphire amplifier (Libra HE, Coherent, Inc.). Pump pulses were depolarized with a quartz-wedge achromatic depolarizer (Thorlabs, DPU-25) before the sample position. The mechanical chopper, synched to the amplifier and operating at half of the amplifier frequency, was used to block half of the pump pulses before the sample. Supercontinuum probe pulses (~200 fs pulse width) were generated by focusing a fraction of the 800 nm amplifier output onto CaF₂ or sapphire plates (3 mm thick). The probe beam was temporally delayed from the pump using a mechanical delay line with a retroreflector. Timeresolved TA spectra (ΔA) were collected with a fiber-coupled multichannel photodiode array spectrometer and plotted as the differential optical density of transmitted probe light after the sample, $\Delta A(\lambda, t) = \mathrm{OD}_{\mathrm{pump}}(\lambda, t) - \mathrm{OD}_{\mathrm{nopump}}(\lambda, t)$. A reference line was monitored to account for fluctuations in the probe beam, and pump-probe delay was scanned at random positions to minimize the potential influence of setup drift or sample degradation effects. TA spectra were measured in a 2 mm path length quartz cuvette (Starna Cells) with continuous stirring using a clean polytetrafluoroethylene-coated magnetic stir bar.

Global Analysis. To deconvolute and analyze time-resolved spectra, global analysis was performed using Glotaran,

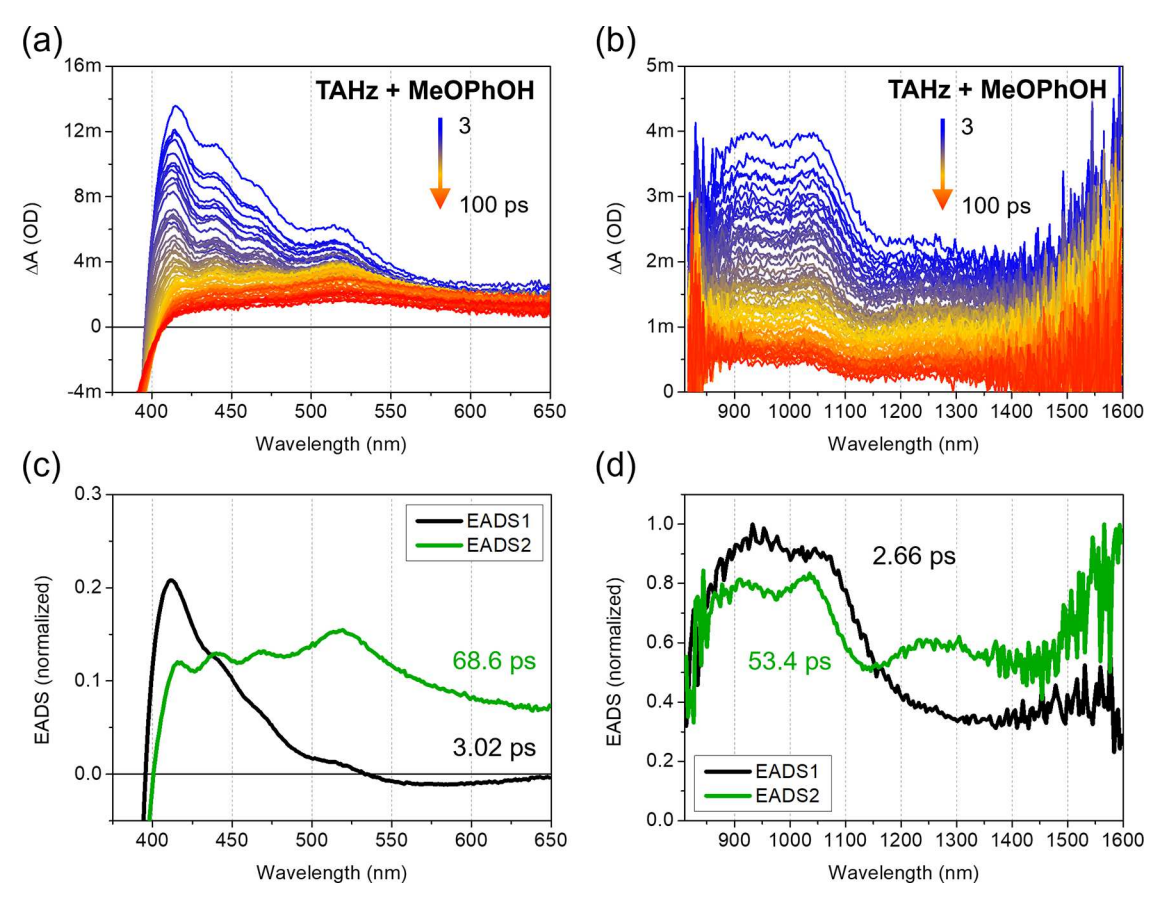


Figure 2. Time-resolved pump–probe spectra and evolution-associated decay spectra (EADS) from global analysis of TAHz (50 μ M) + MeOPhOH (1 M) in toluene with 365 nm pump excitation. Timesteps were log-scale from 3 to 100 ps pump–probe delays. (a, c) Visible wavelength region probe and (b, d) near-IR wavelength region probe. The fitting model was a parallel decay model with two exponential decay functions. Lifetimes of each EADS shown in the figure.

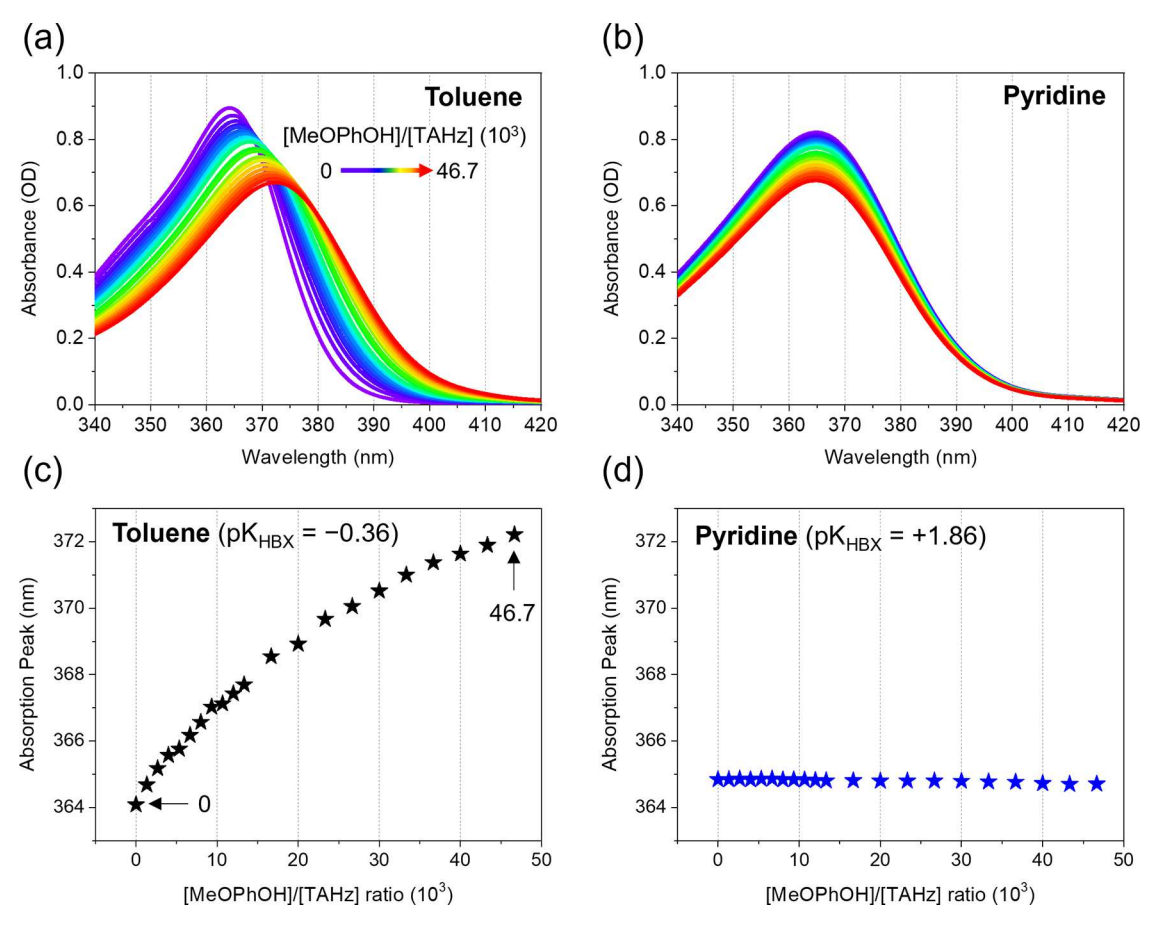
a graphical user interface for the R-package TIMP.⁵² The analysis performed here contained two spectral components, according to the singular value decomposition, each with their respective decay constants. Parallel or sequential two exponential decay models were adopted, as indicated in the figure captions for each global analysis result. No parameters were constrained.

Computational Studies. Density functional theory (DFT) and time-dependent DFT (TD-DFT) calculations were performed with the B3LYP functional, Grimme's dispersion correction (D3), and the cc-pVDZ basis set. The calculations were performed with the TURBOMOLE program package⁵³ using the resolution-of-the-identity (RI) approximation.

■ RESULTS AND DISCUSSION

Figure 1a summarizes the Hz photochemistry studied in this paper. Hz derivatives can form a hydrogen-bonded intermolecular complex with H-atom donor substrates, and upon photoexcitation, the complex undergoes an excited-state intermolecular PCET photoreaction, which generates radicalpair products. The hydrogen-bonding interaction induces a shift of the UV—vis absorption spectrum of Hz derivatives (Figure 1b) due to changes in the vertical excitation energy of the excited states associated with the Hz core. The excited-state PCET in the hydrogen-bonded complex also quenches photoluminescence by providing an additional nonradiative decay channel (Figure 1c).

Figure 2 shows TA data and global analysis results of TAHz with MeOPhOH as the substrate. Previously, with other lessreactive phenolic substrates (Figure S3), we have measured and assigned two evolution-associated decay spectra (EADS): one with a fast time constant is attributed to hydrogen-bonded TAHz and one with a slower time constant to free TAHz in the solution. Those results were primarily obtained from timeresolved photoluminescence (TR-PL)⁴⁹ and supported by TA spectroscopy.⁵⁰ Based on our previous analysis, and by comparing the spectral signatures of various TAHz:R-PhOH complexes, we attributed the fast EADS component (EADS1) in Figure 2 to the excited state of hydrogen-bonded TAHz, with a residual contribution from free TAHz. While our prior PL measurements did not allow us to evaluate the appearance of photochemical products, in our TA measurements here, we can now identify a new slow EADS component (EADS2) with three distinctly identifiable peaks emerging, one at 520 nm and two at 1250 and 1600 nm, for TAHz:MeOPhOH. These new peaks do not appear for TAHz without any phenolic substrate (Figure S2), which exhibits two EADS attributable to vibronic relaxation following the S_n state excitation and decay of the S_1 state. The new peaks are also unresolvable for less-reactive R-PhOHs (Figure S3), therein two EADS represent contributions from free and hydrogen-bonded TAHz. Since the barrierless PCET reaction and efficient radical-pair product generation are achieved only with the most reactive substrate, MeOPhOH, 49 we postulated that these three distinct peaks originate from absorption of radical products. That is, the



pubs.acs.org/JPCB

Figure 3. UV-vis absorption spectra of TAHz with the addition of MeOPhOH ([MeOPhOH]/[TAHz] = $0-46.7 \times 10^3$) in (a) toluene or (b) pyridine solvent. (c, d) Absorption peak shifts with the addition of MeOPhOH for toluene solution, but not for pyridine solution. Peak positions were determined from fitting with a Gaussian peak-fitting function.

PCET reaction of the TAHz:MeOPhOH complex generates a sufficiently high concentration of TAHzH $^{\bullet}$ and MeOPhO $^{\bullet}$ radical pair to be readily detected over the excited-state absorption background of the closed-shell species. Considering that the absorption of the MeOPhO $^{\bullet}$ radical is limited to the near-UV range ($\lambda \leq 450$ nm), ^{55,56} these three new induced absorption peaks were attributed to the TAHzH $^{\bullet}$ radical absorption.

By using 1,4-dimethoxybenzene (DMB) as a substrate with an oxidation potential analogous to MeOPhOH, but without transferrable hydrogen atoms, 49 the substrate can only transfer an electron but not a proton to TAHz after photoexcitation of the latter, generating a TAHz - radical anion product instead of the TAHzH radical. Applying global analysis to these TA results for TAHz with DMB (Figure S4) indicates that TAHz exhibits three new absorption peaks, one at 525 nm and two at 1250/1550 nm, as expected for the reduced form of TAHz that results in the TAHzH signatures discussed above. The reduced forms of polymeric carbon nitrides, which comprise Hz monomeric units, exhibit broad absorption features throughout the Vis-NIR region, beginning at roughly 650 nm.⁵⁷⁻⁶¹ It has been observed both computationally and experimentally that TAHz can serve as a well-defined molecular model of carbon nitrides. 40,54 Thus, the emergence of a new absorption feature in the spectral range near 520 nm for the reduced form of TAHz is perhaps unsurprising. Spectroelectrochemical measurements also recapitulated the emergence of spectral peaks at roughly 500, 1300, and 1600

nm for the electrochemical reduction of TAHz (Figure S5). That is, electrochemically reducing TAHz in solution yields peaks that corroborate our assignments of the peaks at 525, 1250, and 1550 nm as the absorption peaks for the reduced forms of TAHz. Similarities among the absorption peak positions for the anionic radical form and the neutral, protonated radical counterpart of chromophores have been observed for several other small molecules, such as 2,4-dihydroxybenzoic acid,⁶² N-methyl-4,4'-bipyridine,⁶³ and adenine—tyrosine complex.⁶⁴ For TAHzH• and TAHz•, however, the two product molecules of similar spectral signatures exhibit significant differences in kinetics and response to radical quenchers, as discussed below.

The excited-state PCET and radical product generation processes occur in a preassociated, hydrogen-bonded intermolecular complex, TAHz:MeOPhOH. On the other hand, the interaction of excited-state TAHz and DMB occurs in a collisional reaction wherein only an electron, but no proton, is transferred from DMB to TAHz, since DMB has no readily abstractable H atom and cannot efficiently form a hydrogen bond to TAHz. This difference in reaction kinetics is clearly seen in the time-resolved profile of the 520–525 nm peaks in our TA measurements (Figure S6). In the TAHz:MeOPhOH hydrogen-bonded complex, the near-zero reaction barrier in the excited state leads to ultrafast PCET, which is reflected in the near-immediate rise of the 520 nm peak in the ΔA data. In the TAHz + DMB reaction, however, the electron-transfer process is limited by diffusional collisions. As a result, the rise

time of the 525 nm peak is substantially slower than in the preassociated, TAHz:MeOPhOH case. In addition to the differences in the rise times, the decay kinetics also show a considerable difference: the TAHzH (TAHz:MeOPhOH) signal dies out on a relatively short time scale (\sim 130 ps), while the TAHz*- (TAHz + DMB) signal decays on a longer time scale of a few nanosecond. A more remarkable difference occurs when the solvent environment includes the radical quencher, styrene.65-67 The TAHzH• radical is effectively quenched by styrene molecules. Adding styrene indeed greatly accelerates the decay of the 520 nm signal in the TAHz:MeOPhOH sample (lifetime changed to < 50 ps). The TAHz*- signal, on the other hand, exhibits virtually no change in decay kinetics when styrene is added to the TAHz + DMB sample solution (Figure S6). DFT calculations indicate that H transfer from TAHzH to styrene is an exothermic process. However, for the TAHz*- + styrene system, DFT/ TD-DFT calculations indicate that the excess electron on the TAHz - radical anion is not transferred to styrene once it is photochemically formed (Figure S6). These computational results suggest that styrene can quench the TAHzH* radical by readily accepting H[•], but it cannot quench the TAHz^{•-} radical anion by accepting an electron.

The observed differences in experimental, as well as computational, results support the hypothesis that intermolecular PCET in a preassociated complex generates the TAHzH radical in the MeOPhOH case, while collisioncontrolled electron transfer generates the TAHz*- radical anion in the DMB case. This disparity leads to different timeresolved profiles of the TA signals despite similarities in the line shapes of the TA spectra for both the TAHz:MeOPhOH and TAHz + DMB cases. In other words, these two systems yield different photochemical products with different reaction kinetics but with similar spectral fingerprints. Experimental results where H⁺ was added to TAHz with a Brønsted-Lowry acid also support this hypothesis (Figure S7). Adding sequentially increasing amounts of trifluoroacetic acid (TFA) to the TAHz + DMB sample solution retains the ~520 nm peak in the TA data but accelerates its decay rate. As more TFA is added, the decay rate of this feature approaches that for the PCET and TAHzH• generation case (TAHz:MeOPhOH). Presumably, this decay rate approaching the TAHzH case occurs via H+ transfer from TFA and excited-state e- transfer from DMB to TAHz. These results help to contextualize the different kinetics that we observe in the excited-state intermolecular PCET (MeOPhOH) and pure electron-transfer (DMB) cases to yield different photoreduced forms of the TAHz chromophore.

Control of PCET reactivity and radical product generation has been of great importance in understanding the fundamentals of PCET-driven photochemistry, as well as facilitating its applications. 4,5,68 Since TAHz:MeOPhOH is a hydrogen-bonded molecular complex and its photochemistry involves an intermolecular PCET process, we hypothesized that it may be possible to control the radical generation by manipulating the hydrogen-bonding interaction between TAHz and substrate. In order to test this hypothesis, we explored whether one can control the formation of hydrogenbonded complexes of phenol with TAHz by utilizing solvents with different propensities to outcompete the hydrogen bonding of TAHz with MeOPhOH. 69,70 We can quantify the tendency of solvents to form hydrogen bonds based on the hydrogen-bond-acceptor strength parameter pK_{HBX} ($pK_{HBX}(X)$

 $\equiv \log_{10}\{[X:4\text{-fluorophenol}][X]^{-1}[4\text{-fluorophenol}]^{-1}\}$ in carbon tetrachloride). 71,72 Figure 3 shows a series of absorption spectra and peak shifts of TAHz with increasing concentration of MeOPhOH, in toluene (i.e., the least hydrogen-bondaccepting solvent in this study) or pyridine (the most hydrogen-bond-accepting solvent). TAHz with MeOPhOH in toluene exhibits a significant red shift of its absorption peak (bright $\pi\pi^*$ transition of TAHz) due to the hydrogen-bonding interaction between TAHz and MeOPhOH. However, there is no readily discernable absorption peak shift when TAHz and MeOPhOH are dissolved in pyridine, the most aggressive hydrogen-bond-accepting solvent with the highest p K_{HBX} value among the solvents used in this work. Comparing a series of solvents with different p $K_{\rm HBX}$ (Figure S8) clearly demonstrates that the extent of absorption peak shift for both bright and dark $\pi\pi^*$ transitions of Hz core follows the hydrogen-bondacceptor strength scale of solvents rather than other solvent parameters such as dielectric constant or viscosity (Table 1).

Table 1. Parameters for Solvents Used in This Work⁷¹⁻⁷³

	dielectric constant	viscosity (cP)	pK_{HBX}
toluene	2.379	0.560	-0.36
anisole	4.30	1.056	-0.07
benzonitrile	25.9	1.267	+0.80
pyridine	13.260	0.879	+1.86

It is also notable that the N-heterocyclic moiety analogous to the heptazine core, 1,3,5-triazine, for which there is a known literature value for p $K_{\rm HBX}$ of +0.32, lies between the respective values of p K_{HBX} for toluene and pyridine.⁷² Based on p K_{HBX} values, we expect that pyridine will outcompete TAHz to form hydrogen-bonded complexes with the hydroxyl group of the substrate molecule. Thus, these pK_{HBX} values agree with the experimentally observed trend with TAHz in this work: toluene (p $K_{HBX} = -0.36$) cannot interrupt the hydrogenbonding interaction of TAHz:MeOPhOH, while pyridine $(pK_{HBX} = +1.86)$ intercepts almost all MeOPhOH molecules from hydrogen bonding with the triazinic (p $K_{HBX} = +0.32$) nitrogen of the heptazine core of TAHz. DFT calculations confirm that hydrogen bonding between pyridine and MeOPhOH is energetically more favorable than hydrogen bonding between TAHz and MeOPhOH. This theoretical result suggests that pyridine is capable of intercepting the preponderance of available MeOPhOH and is consistent with our experimental observation that the formation of TAHz:-MeOPhOH complexes is suppressed in pyridine (Figure S9). Based on these observations, we conclude that the intermolecular hydrogen-bonding interaction between TAHz and the MeOPhOH substrate can be controlled by hydrogenbond interfering solvent environments.

Since the photoinduced intermolecular PCET reaction of TAHz only occurs in the hydrogen-bonded, preassociated TAHz:MeOPhOH complex, control of the hydrogen-bonding interaction should allow the manipulation of the excited-state intermolecular PCET and radical product generation processes. Experimentally, this control of the excited-state PCET reaction can be probed with the spectroscopic signatures of the TAHzH• product known from TA spectroscopy (Figure 2). Figures 4 and S10 show time-resolved ΔA spectra of TAHz with MeOPhOH substrate in solvents of different hydrogenbond-acceptor strengths. Apparently, the amplitude of the 520 nm peak, one of three spectral signatures of TAHzH*,

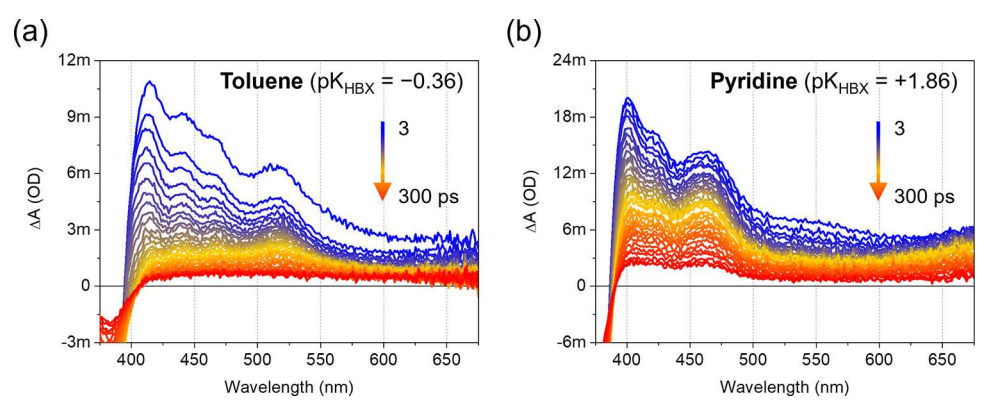


Figure 4. Time-resolved pump—probe spectra of TAHz (50 uM) with MeOPhOH (1 M) in (a) toluene or (b) pyridine solvent. Timesteps were log-scale from 3 to 300 ps pump—probe delays. Pump wavelength was 365 nm.

decreases as pK_{HBX} of the solvent increases. This trend suggests that the more the hydrogen bonding between TAHz and MeOPhOH is disrupted by the interfering solvent, the less excited-state intermolecular PCET reaction and radical product generation occurs. Global analysis results of the TA data (Figure S12) support this assessment: the amplitude of the 520 nm peak decreases as solvent pK_{HBX} increases. It is noteworthy that for the strongest hydrogen-bond-accepting solvents (e.g., pyridine), where almost all of the hydrogen bonding between TAHz and MeOPhOH is suppressed (note that the steady-state absorption shift of TAHz is near-zero in Figure 3b), the spectral shape of ΔA signal of the TAHz + MeOPhOH sample in pyridine is virtually identical to the TAHz-only case. We attribute this TA signal suppression to the fact that preassociation of TAHz with MeOPhOH cannot occur and, therefore, no excited-state intermolecular PCET reaction proceeds between TAHz and MeOPhOH (vide infra). We note that hydrogen-bonded dyads of pyridine and MeOPhOH (Pyr:MeOPhOH) can act as a quencher for photoexcited TAHz through a different type of collision-based, multisite PCET reaction where the process involves e⁻ and H⁺ transfer from MeOPhOH to TAHz and pyridine respectively and generates TAHz*- + MeOPhO* + Pyr-H* products, similarly to the quenching of triplet fullerenes observed by Linschitz and co-workers. The small shoulder-like signal around 520-550 nm at very early pump-probe delay in Figure 4b may arise from the generation of TAHz - radical anion due to this collision-based process. However, it appears that if this process occurs, the reaction does not produce a sizable population of long-lived radical or charged species that can be resolved in our experiment. This lack of signal is in contrast to the PCET process involved in transferring a hydrogen atom to TAHz in hydrogen-bonded TAHz:MeOPhOH complexes in toluene. The TA data in Figure 4b shows that the shoulder-like signal exhibits a significantly less-prominent peak, which decays quickly within a few picoseconds and the resulting spectral shape of the ΔA signal of TAHz + MeOPhOH in pyridine is virtually identical to the TAHz-only case.

On the other hand, the reaction kinetics for collisional, electron-only transfer and TAHz^{•-} radical anion generation with the DMB substrate should be strongly influenced by the electrostatic environment of the system, which, for the purposes of our study, we will quantitatively evaluate based on the bulk dielectric constants of the solvents. Time-resolved TA data (Figure S11) and global analysis (Figure S13) show that the spectral signature of the TAHz^{•-} radical anion (525)

nm) does not change with solvent pK_{HBX} , but rather changes with solvent dielectric constants; generally, we observe smaller amplitude and faster decay of the 525 nm peak in solvents with higher dielectric constants. It is noteworthy that the decay of the TAHz - signal (525 nm peak), which represents an electron back-transfer process from TAHz*- to DMB+, has a shorter lifetime in solvents with higher dielectric constants (e.g., pyridine and benzonitrile) than in those whose dielectric constants are lower (e.g., toluene and anisole). Solvents with higher dielectric constants are commonly regarded to impart a stabilizing effect on the free energy of charge-separated states compared to charge-neutral states. 76 The electron back-transfer process in the TAHz^{•-} + DMB⁺ system may be in the Marcus inverted regime, meaning that the energetically stabilized charge-separated state can result in enhanced charge recombination to the charge-neutral ground state,⁷⁷ although quantitatively evaluating this back-transfer process lies beyond the scope of the present study.

Figure 5 shows a schematic diagram summarizing the results obtained in this work. In a hydrogen-bonding inert solvent such as toluene, preassociation of TAHz:MeOPhOH is not disturbed and thus the intermolecular PCET and radical product generation proceed efficiently upon photoexcitation. However, in a hydrogen-bond-intercepting solvent such as pyridine, we observe no appreciable hydrogen bonding between TAHz and MeOPhOH in solution. That is, the preassociated complex with MeOPhOH does not appear to form. Thus, the prompt intermolecular PCET reaction does not proceed with pyridine as the solvent. This molecular picture is strongly supported by the TA spectra shown in Figure 5, where only TAHz + MeOPhOH in toluene exhibits the characteristic ΔA peak at 520 nm, while TAHz + MeOPhOH in pyridine shows a spectral shape that is nearly identical to the TAHz-only case.

CONCLUSIONS

In this work, we investigated Hz photochemistry with a Hatom donor substrate through spectroscopic analysis of the model Hz derivative, TAHz, and substituted phenols. We applied time-resolved TA spectroscopy measurements for TAHz:MeOPhOH complexes to recover spectral signatures of the radical product, TAHzH•. The spectral signatures of TAHzH• allow us to analyze the reaction dynamics of excited-state PCET and radical product generation processes. Based on these assignments, we investigated the role of hydrogen bonding in the preassociation and excited-state PCET reaction

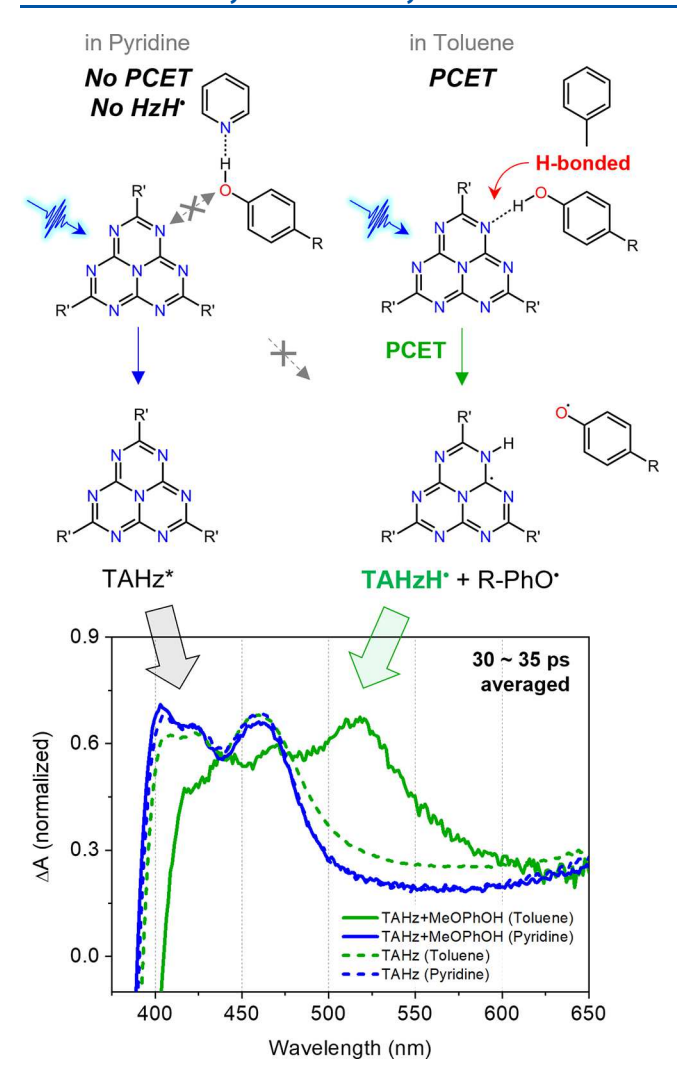


Figure 5. (Top) Schematic diagram of TAHz:MeOPhOH photochemistry. In the least hydrogen-bond-accepting solvent, toluene, TAHz forms a hydrogen-bonded complex with R-PhOH substrates, undergoing intermolecular PCET reaction upon near-UV photoexcitation and generating a radical-pair product. In the most hydrogen-bond-accepting solvent, pyridine, TAHz cannot form a hydrogen-bonded complex with R-PhOH and, consequently, cannot undergo intermolecular PCET reaction. (Bottom) Normalized ΔA spectra from TA measurement of TAHz (50 uM) only (solid line) and with MeOPhOH (1 M) sample (dashed line) in toluene (green) and pyridine (blue) solvent. While the 520 nm peak is clearly visible in TAHz + MeOPhOH in the toluene case, the peak is completely absent in TAHz + MeOPhOH in the pyridine and TAHz-only cases in both solvents. Note that in pyridine solvent, where almost all of the hydrogen bonds between TAHz and MeOPhOH are interrupted by pyridine solvent molecules, the ΔA spectral shapes from TAHz-only and TAHz + MeOPhOH samples are near-identical. ΔA spectra are averaged from 30 to 35 ps delay time between pump and probe.

of the TAHz:substrate complex by controlling intermolecular hydrogen-bonding interaction of the complex and tracking the identified TAHzH $^{\bullet}$ product spectral signature. We demonstrated that the preassociation of TAHz and the substrate molecule plays a critical role in intermolecular PCET photochemistry of Hz derivatives. Our results also indicate that the excited-state PCET reaction of Hz derivatives can be systematically controlled with solvents of various hydrogen-bond-acceptor strength, parameterized by p $K_{\rm HBX}$. Steady-state absorption and time-resolved TA measurements indicate that

the solvent with the highest value of pK_{HBX} interrupts hydrogen bonding of the TAHz:MeOPhOH intermolecular complex. This interruption suppresses the excited-state PCET reaction and radical product generation. We also compared the PCET photochemistry of the TAHz:MeOPhOH complex with collisional electron transfer involving no proton transfer to form the TAHz• radical anion, using DMB as the substrate. In that case, reaction dynamics appear to be governed by the dielectric properties of the solvent—evaluated based on the bulk dielectric constant—rather than the hydrogen-bond-accepting strength of the solvent.

Understanding the details of intra/intermolecular PCET and manipulating the reaction may provide future insight into optimizing PCET processes for energy conversion systems, ranging from photoactive carbon nitrides to various photocatalysts and electrocatalysts. For example, we observed in this work that one viable way of fine-tuning photoinduced PCET reactions may be to manipulate intermolecular hydrogenbonding interactions between a photoactive molecule and its substrate. These results suggest that the external interaction of the solvent can control the preassociation of reactants and, ultimately, influences the excited-state PCET reaction of the preassociated complex and radical product generation. The spectral signatures of reduced forms of TAHz (TAHzH and TAHz - assigned in this work will also facilitate future indepth analysis of Hz photochemistry and carbon nitride photoactivity in general, and photocatalytic water splitting, 32,35 particularly with regard to the two-electron water oxidation process, ^{38,40} and related photogenerated charge storage behavior. ^{36,37} We anticipate that our results can be utilized to tailor intermolecular or even intramolecular PCET reactions not just by chemically functionalizing the Hz chromophore but also by controlling the surrounding molecular environment. Similar to highly efficient biological catalytic systems with sophisticated hydrogen-bonding networks, 79-81 our work suggests potential design strategies for tuning the molecular environment of Hz derivatives using chemically modified pendant groups^{82,83} or supramolecular chemistry. 84,85 These modifications, for example, may be used to block solvent interference. Such an approach could be used to induce stronger interactions at desired orientations between the Hz chromophore and a substrate of interest. A similar avenue could be particularly compelling for attempting to oxidize water to enhance excited-state PCET and the overall water splitting reaction efficiency.

ASSOCIATED CONTENT

5 Supporting Information

The Supporting Information is available free of charge at https://pubs.acs.org/doi/10.1021/acs.jpcb.3c01397.

Details of concentration-dependent UV—vis absorption measurements, global analysis of time-resolved spectroscopy data of TAHz with R-PhOH and DMB substrates, spectroelectrochemical characterization of anionic radical form of TAHz, results from radical quencher and Brønsted—Lowry acid control experiments, solvent dependence of steady-state and time-resolved spectroscopy of TAHz with MeOPhOH, and computational analysis (PDF)

AUTHOR INFORMATION

Corresponding Author

Cody W. Schlenker — Department of Chemistry, University of Washington, Seattle, Washington 98195, United States; Molecular Engineering & Sciences Institute, University of Washington, Seattle, Washington 98195-1652, United States; Clean Energy Institute, University of Washington, Seattle, Washington 98195-1653, United States; orcid.org/0000-0003-3103-402X; Email: schlenk@uw.edu

Authors

Doyk Hwang — Department of Chemistry, University of Washington, Seattle, Washington 98195, United States; orcid.org/0000-0001-5275-0354

Liam M. Wrigley – Department of Chemistry, University of Washington, Seattle, Washington 98195, United States

Micah Lee – Department of Chemistry, University of Washington, Seattle, Washington 98195, United States

Andrzej L. Sobolewski – Institute of Physics, Polish Academy of Sciences, PL-02-668 Warsaw, Poland; orcid.org/0000-0001-5718-489X

Wolfgang Domcke — Department of Chemistry, Technical University of Munich, D-85747 Garching, Germany; orcid.org/0000-0001-6523-1246

Complete contact information is available at: https://pubs.acs.org/10.1021/acs.jpcb.3c01397

Author Contributions

*D.H. and L.M.W. contributed equally to this work. D.H., L.M.W., and C.W.S. conceived this research work. L.M.W. synthesized materials used in this study and conducted steady-state spectroscopy and spectroelectrochemical measurement with the help from M.L. D.H. conducted time-resolved spectroscopic measurement and global analysis of data. A.L.S. and W.D. conducted the computational analysis. D.H., L.M.W., and C.W.S. wrote the manuscript. All authors have read and given approval to the final version of the manuscript.

Notes

The authors declare no competing financial interest.

ACKNOWLEDGMENTS

This work is based on research that was supported in part by the Washington Research Foundation and the University of Washington Clean Energy Institute (CEI). Part of this work was conducted at the Molecular Analysis Facility, a National Nanotechnology Coordinated Infrastructure (NNCI) site at the University of Washington, which is supported in part by funds from the National Science Foundation (awards NNCI-2025489, NNCI-1542101), the Molecular Engineering & Sciences Institute, and the Clean Energy Institute. C. W. S. acknowledges that a portion of this material is based upon work supported by the US National Science Foundation (NSF) under Grant No. [1846480].

REFERENCES

- (1) Weinberg, D. R.; Gagliardi, C. J.; Hull, J. F.; Murphy, C. F.; Kent, C. A.; Westlake, B. C.; Paul, A.; Ess, D. H.; McCafferty, D. G.; Meyer, T. J. Proton-coupled electron transfer. *Chem. Rev.* **2012**, *112*, 4016–4093.
- (2) Migliore, A.; Polizzi, N. F.; Therien, M. J.; Beratan, D. N. Biochemistry and theory of proton-coupled electron transfer. *Chem. Rev.* **2014**, *114*, 3381–3465.

- (3) Lennox, J. C.; Kurtz, D. A.; Huang, T.; Dempsey, J. L. Excited-state proton-coupled electron transfer: different avenues for promoting proton/electron movement with solar photons. *ACS Energy Lett.* **2017**, *2*, 1246–1256.
- (4) Goyal, P.; Hammes-Schiffer, S. Tuning the ultrafast dynamics of photoinduced proton-coupled electron transfer in energy conversion processes. ACS Energy Lett. 2017, 2, 512–519.
- (5) Darcy, J. W.; Koronkiewicz, B.; Parada, G. A.; Mayer, J. M. A continuum of proton-coupled electron transfer reactivity. *Acc. Chem. Res.* **2018**, *51*, 2391–2399.
- (6) Nocera, D. G. Proton-Coupled Electron Transfer: The Engine of Energy Conversion and Storage. *J. Am. Chem. Soc.* **2022**, *144*, 1069–1081
- (7) Gentry, E. C.; Knowles, R. R. Synthetic applications of proton-coupled electron transfer. *Acc. Chem. Res.* **2016**, *49*, 1546–1556.
- (8) Hoffmann, N. Proton-Coupled Electron Transfer in Photoredox Catalytic Reactions. *Eur. J. Org. Chem.* **2017**, 2017, 1982–1992.
- (9) Gagliardi, C. J.; Vannucci, A. K.; Concepcion, J. J.; Chen, Z.; Meyer, T. J. The role of proton coupled electron transfer in water oxidation. *Energy Environ. Sci.* **2012**, *5*, 7704–7717.
- (10) Thammavongsy, Z.; Mercer, I. P.; Yang, J. Y. Promoting proton coupled electron transfer in redox catalysts through molecular design. *Chem. Commun.* **2019**, *55*, 10342–10358.
- (11) Markle, T. F.; Mayer, J. M. Concerted proton—electron transfer in pyridylphenols: The importance of the hydrogen bond. *Angew. Chem., Int. Ed.* **2008**, *47*, 738–740.
- (12) Alligrant, T. M.; Alvarez, J. C. The role of intermolecular hydrogen bonding and proton transfer in proton-coupled electron transfer. *J. Phys. Chem. C* **2011**, *115*, 10797–10805.
- (13) Eisenhart, T. T.; Dempsey, J. L. Photo-induced proton-coupled electron transfer reactions of acridine orange: comprehensive spectral and kinetics analysis. *J. Am. Chem. Soc.* **2014**, *136*, 12221–12224.
- (14) Concepcion, J. J.; Brennaman, M. K.; Deyton, J. R.; Lebedeva, N. V.; Forbes, M. D.; Papanikolas, J. M.; Meyer, T. J. Excited-state quenching by proton-coupled electron transfer. *J. Am. Chem. Soc.* **2007**, *129*, 6968–6969.
- (15) Pizano, A. A.; Yang, J. L.; Nocera, D. G. Photochemical tyrosine oxidation with a hydrogen-bonded proton acceptor by bidirectional proton-coupled electron transfer. *Chem. Sci.* **2012**, *3*, 2457–2461.
- (16) Kuss-Petermann, M.; Wenger, O. S. Photoacid Behavior versus Proton-Coupled Electron Transfer in Phenol—Ru (bpy) 32+ Dyads. *J. Phys. Chem. A* **2013**, *117*, 5726—5733.
- (17) Wenger, O. S. Proton-coupled electron transfer with photo-excited metal complexes. *Acc. Chem. Res.* **2013**, *46*, 1517–1526.
- (18) Dongare, P.; Bonn, A. G.; Maji, S.; Hammarström, L. Analysis of Hydrogen-Bonding Effects on Excited-State Proton-Coupled Electron Transfer from a Series of Phenols to a Re (I) Polypyridyl Complex. J. Phys. Chem. C 2017, 121, 12569–12576.
- (19) Miller, D. C.; Tarantino, K. T.; Knowles, R. R. Proton-Coupled Electron Transfer in Organic Synthesis: Fundamentals, Applications, and Opportunities. In *Hydrogen Transfer Reactions: Reductions and Beyond*; Guillena, G.; Ramón, D. J., Eds.; Springer International Publishing, 2016; pp 145–203.
- (20) Dang, H. T.; Haug, G. C.; Nguyen, V. T.; Vuong, N. T.; Nguyen, V. D.; Arman, H. D.; Larionov, O. V. Acridine photocatalysis: insights into the mechanism and development of a dual-catalytic direct decarboxylative conjugate addition. *ACS Catal.* **2020**, *10*, 11448–11457.
- (21) Berg, N.; Bergwinkl, S.; Nuernberger, P.; Horinek, D.; Gschwind, R. M. Extended Hydrogen Bond Networks for Effective Proton-Coupled Electron Transfer (PCET) Reactions: The Unexpected Role of Thiophenol and Its Acidic Channel in Photocatalytic Hydroamidations. *J. Am. Chem. Soc.* 2021, 143, 724–735.
- (22) Reece, S. Y.; Nocera, D. G. Proton-coupled electron transfer in biology: results from synergistic studies in natural and model systems. *Annu. Rev. Biochem.* **2009**, *78*, 673–699.
- (23) Hammarström, L.; Styring, S. Proton-coupled electron transfer of tyrosines in Photosystem II and model systems for artificial

- photosynthesis: the role of a redox-active link between catalyst and photosensitizer. *Energy Environ. Sci.* **2011**, *4*, 2379–2388.
- (24) Chai, J.; Zheng, Z.; Pan, H.; Zhang, S.; Lakshmi, K.; Sun, Y.-Y. Significance of hydrogen bonding networks in the proton-coupled electron transfer reactions of photosystem II from a quantum-mechanics perspective. *Phys. Chem. Chem. Phys.* **2019**, 21, 8721–8728.
- (25) Young, E. R.; Rosenthal, J.; Hodgkiss, J. M.; Nocera, D. G. Comparative PCET Study of a Donor– Acceptor Pair Linked by Ionized and Nonionized Asymmetric Hydrogen-Bonded Interfaces. *J. Am. Chem. Soc.* **2009**, *131*, 7678–7684.
- (26) Kucheryavy, P.; Khatmullin, R.; Mirzakulova, E.; Zhou, D.; Glusac, K. D. Photoinduced electron transfer in naphthalimide-pyridine systems: effect of proton transfer on charge recombination efficiencies. *J. Phys. Chem. A* **2011**, *115*, 11606–11614.
- (27) Lymar, S. V.; Ertem, M. Z.; Lewandowska-Andralojc, A.; Polyansky, D. E. Role of Hydrogen Bonding in Photoinduced Electron—Proton Transfer from Phenols to a Polypyridine Ru Complex with a Proton-Accepting Ligand. *J. Phys. Chem. Lett.* **2017**, 8, 4043—4048.
- (28) Venkatesan, M.; Mandal, H.; Chakali, M.; Bangal, P. R. Excited-State Quenching of Porphyrins by Hydrogen-Bonded Phenol-Pyridine Pair: Evidence of Proton-Coupled Electron Transfer§. *J. Phys. Chem.* C 2019, 123, 23342–23351.
- (29) Clare, L. A.; Pham, T. D.; Rafou, L. A.; Buenaventura, A. G.; Scott, T. R.; Mikhaylova, V.; Smith, D. K. The role of H-bonding in nonconcerted proton-coupled electron transfer: explaining the voltammetry of phenylenediamines in the presence of weak bases in acetonitrile. *J. Phys. Chem. C* 2019, 123, 23390–23402.
- (30) Rono, L. J.; Yayla, H. G.; Wang, D. Y.; Armstrong, M. F.; Knowles, R. R. Enantioselective photoredox catalysis enabled by proton-coupled electron transfer: development of an asymmetric azapinacol cyclization. *J. Am. Chem. Soc.* **2013**, *135*, 17735–17738.
- (31) Miller, D. C.; Choi, G. J.; Orbe, H. S.; Knowles, R. R. Catalytic olefin hydroamidation enabled by proton-coupled electron transfer. *J. Am. Chem. Soc.* **2015**, *137*, 13492–13495.
- (32) Wang, X.; Blechert, S.; Antonietti, M. Polymeric graphitic carbon nitride for heterogeneous photocatalysis. *Acs Catal.* **2012**, *2*, 1596–1606.
- (33) Cao, S.; Low, J.; Yu, J.; Jaroniec, M. Polymeric photocatalysts based on graphitic carbon nitride. *Adv. Mater.* **2015**, *27*, 2150–2176.
- (34) Ong, W.-J.; Tan, L.-L.; Ng, Y. H.; Yong, S.-T.; Chai, S.-P. Graphitic carbon nitride (g-C3N4)-based photocatalysts for artificial photosynthesis and environmental remediation: are we a step closer to achieving sustainability? *Chem. Rev.* **2016**, *116*, 7159–7329.
- (35) Wang, Y.; Vogel, A.; Sachs, M.; Sprick, R. S.; Wilbraham, L.; Moniz, S. J.; Godin, R.; Zwijnenburg, M. A.; Durrant, J. R.; Cooper, A. I.; Tang, J. Current understanding and challenges of solar-driven hydrogen generation using polymeric photocatalysts. *Nat. Energy* **2019**, *4*, 746–760.
- (36) Mazzanti, S.; Savateev, A. Emerging concepts in carbon nitride organic photocatalysis. *ChemPlusChem* **2020**, *85*, 2499–2517.
- (37) Lau, V. W. h.; Lotsch, B. V. A Tour-Guide through Carbon Nitride-Land: Structure-and Dimensionality-Dependent Properties for Photo (Electro) Chemical Energy Conversion and Storage. *Adv. Energy Mater.* **2021**, No. 2101078.
- (38) Liu, J.; Liu, Y.; Liu, N.; Han, Y.; Zhang, X.; Huang, H.; Lifshitz, Y.; Lee, S.-T.; Zhong, J.; Kang, Z. Metal-free efficient photocatalyst for stable visible water splitting via a two-electron pathway. *Science* **2015**, 347, 970–974.
- (39) Ehrmaier, J.; Karsili, T. N.; Sobolewski, A. L.; Domcke, W. Mechanism of photocatalytic water splitting with graphitic carbon nitride: photochemistry of the heptazine—water complex. *J. Phys. Chem. A* **2017**, *121*, 4754–4764.
- (40) Domcke, W.; Sobolewski, A. L.; Schlenker, C. W. Photo-oxidation of water with heptazine-based molecular photocatalysts: Insights from spectroscopy and computational chemistry. *J. Chem. Phys.* **2020**, *153*, No. 100902.

- (41) Huang, X.; Domcke, W. Ab Initio Nonadiabatic Surface-Hopping Trajectory Simulations of Photocatalytic Water Oxidation and Hydrogen Evolution with the Heptazine Chromophore. *J. Phys. Chem. A* **2021**, *125*, 9917–9931.
- (42) Ullah, N.; Chen, S.; Zhao, Y.; Zhang, R. Photoinduced Water-Heptazine Electron-Driven Proton Transfer: Perspective for Water Splitting with g-C₃N₄. *J. Phys. Chem. Lett.* **2019**, *10*, 4310–4316.
- (43) You, P.; Lian, C.; Chen, D.; Xu, J.; Zhang, C.; Meng, S.; Wang, E. Nonadiabatic Dynamics of Photocatalytic Water Splitting on A Polymeric Semiconductor. *Nano Lett.* **2021**, *21*, 6449–6455.
- (44) Ma, H.; Zhang, X.; Jin, F.; Zhou, H.; Zhang, J.; Ma, Y. Crucial roles of triazinic-N=O and C=O groups in photocatalytic water splitting on graphitic carbon nitride. *J. Mater. Chem. A* **2021**, *9*, 5522–5532.
- (45) Lau, V.-h.; Moudrakovski, I.; Botari, T.; Weinberger, S.; Mesch, M. B.; Duppel, V.; Senker, J.; Blum, V.; Lotsch, B. V. Rational design of carbon nitride photocatalysts by identification of cyanamide defects as catalytically relevant sites. *Nat. Commun.* **2016**, *7*, No. 12165.
- (46) Wen, J.; Li, R.; Lu, R.; Yu, A. Photophysics and photocatalysis of melem: a spectroscopic reinvestigation. *Chem. Asian J.* **2018**, *13*, 1060–1066.
- (47) Rabe, E. J.; Corp, K. L.; Sobolewski, A. L.; Domcke, W.; Schlenker, C. W. Proton-coupled electron transfer from water to a model heptazine-based molecular photocatalyst. *J. Phys. Chem. Lett.* **2018**, *9*, 6257–6261.
- (48) Liu, N.; Li, T.; Zhao, Z.; Liu, J.; Luo, X.; Yuan, X.; Luo, K.; He, J.; Yu, D.; Zhao, Y. From Triazine to Heptazine: Origin of Graphitic Carbon Nitride as a Photocatalyst. ACS Omega 2020, 5, 12557–12567.
- (49) Rabe, E. J.; Corp, K. L.; Huang, X.; Ehrmaier, J.; Flores, R. G.; Estes, S. L.; Sobolewski, A. L.; Domcke, W.; Schlenker, C. W. Barrierless Heptazine-Driven Excited State Proton-Coupled Electron Transfer: Implications for Controlling Photochemistry of Carbon Nitrides and Aza-Arenes. *J. Phys. Chem. C* 2019, *123*, 29580–29588.
- (50) Corp, K. L.; Rabe, E. J.; Huang, X.; Ehrmaier, J.; Kaiser, M. E.; Sobolewski, A. L.; Domcke, W.; Schlenker, C. W. Control of Excited-State Proton-Coupled Electron Transfer by Ultrafast Pump-Push-Probe Spectroscopy in Heptazine-Phenol Complexes: Implications for Photochemical Water Oxidation. *J. Phys. Chem. C* **2020**, *124*, 9151–9160.
- (51) Rabe, E. J.; Goldwyn, H. J.; Hwang, D.; Masiello, D. J.; Schlenker, C. W. Intermolecular hydrogen bonding tunes vibronic coupling in heptazine complexes. *J. Phys. Chem. B* **2020**, *124*, 11680–11689.
- (52) Snellenburg, J. J.; Laptenok, S.; Seger, R.; Mullen, K.; Van Stokkum, I. Glotaran: A Java-based graphical user interface for the R package TIMP. *J. Stat. Software* **2012**, *49*, 1–22.
- (53) TURBOMOLE, version 6.3.1, A development of the University of Karlsruhe and Forschungszentrum Karlsruhe GmbH, 1989-2007, TURBOMOLE GmbH since, 2007.
- (54) Hwang, D.; Schlenker, C. W. Photochemistry of carbon nitrides and heptazine derivatives. *Chem. Commun.* **2021**, *57*, 9330–9353.
- (55) Shukla, D.; Schepp, N.; Mathivanan, N.; Johnston, L. Generation and spectroscopic and kinetic characterization of methoxy-substituted phenoxyl radicals in solution and on paper. *Can. J. Chem.* **1997**, *75*, 1820–1829.
- (56) Tonokura, K.; Ogura, T.; Koshi, M. Near-UV absorption spectrum of the phenoxyl radical and kinetics of its reaction with CH₃. *J. Phys. Chem. A* **2004**, *108*, 7801–7805.
- (57) Corp, K. L.; Schlenker, C. W. Ultrafast Spectroscopy Reveals Electron-Transfer Cascade That Improves Hydrogen Evolution with Carbon Nitride Photocatalysts. *J. Am. Chem. Soc.* **2017**, *139*, 7904–7912.
- (58) Lau, V. W. h.; Klose, D.; Kasap, H.; Podjaski, F.; Pignié, M. C.; Reisner, E.; Jeschke, G.; Lotsch, B. V. Dark photocatalysis: storage of solar energy in carbon nitride for time-delayed hydrogen generation. *Angew. Chem., Int. Ed.* **2017**, *56*, 510–514.
- (59) Savateev, A.; Kurpil, B.; Mishchenko, A.; Zhang, G.; Antonietti, M. A "waiting" carbon nitride radical anion: a charge storage material

- and key intermediate in direct C-H thiolation of methylarenes using elemental sulfur as the "S"-source. *Chem. Sci.* **2018**, *9*, 3584–3591.
- (60) Yang, W.; Godin, R.; Kasap, H.; Moss, B.; Dong, Y.; Hillman, S. A. J.; Steier, L.; Reisner, E.; Durrant, J. R. Electron Accumulation Induces Efficiency Bottleneck for Hydrogen Production in Carbon Nitride Photocatalysts. *J. Am. Chem. Soc.* **2019**, *141*, 11219–11229.
- (61) Markushyna, Y.; Lamagni, P.; Teutloff, C.; Catalano, J.; Lock, N.; Zhang, G.; Antonietti, M.; Savateev, A. Green radicals of potassium poly (heptazine imide) using light and benzylamine. *J. Mater. Chem. A* **2019**, *7*, 24771–24775.
- (62) Anderson, R. F.; Patel, K. B.; Vojnovic, B. Absorption spectra of radical forms of 2, 4-dihydroxybenzoic acid, a substrate for phydroxybenzoate hydroxylase. *J. Biol. Chem.* **1991**, 266, 13086—13090.
- (63) Tyburski, R.; Fohlinger, J.; Hammarstrom, L. Light Driven Electron Transfer in Methylbipyridine/Phenol Complexes Is Not Proton Coupled. *J. Phys. Chem. A* **2018**, *122*, 4425–4429.
- (64) Banyasz, A.; Ketola, T.; Martínez-Fernández, L.; Improta, R.; Markovitsi, D. Adenine radicals generated in alternating AT duplexes by direct absorption of low-energy UV radiation. *Faraday Discuss.* **2018**, 207, 181–197.
- (65) Walling, C.; Mayo, F. R. The effect of substitution on the reactivity of the styrene double bond towards free-radical attack: the nature of the "alternating effect" in copolymerisation. *Discuss. Faraday Soc.* 1947, 2, 295–303.
- (66) Moad, G.; Rizzardo, E.; Solomon, D. H. Selectivity of the reaction of free radicals with styrene. *Macromolecules* **1982**, *15*, 909–914.
- (67) Guo, X.-C.; Chen, Q.-Y. The first example of addition reactions of sterically hindered terminal olefins, α -substituted styrenes, with perfluoroalkyl iodides initiated by sodium dithionite. *J. Fluorine Chem.* **1999**, 93, 81–86.
- (68) Rosenthal, J.; Nocera, D. G. Role of proton-coupled electron transfer in O–O bond activation. *Acc. Chem. Res.* **2007**, *40*, 543–553.
- (69) Jin, Y. J.; Aoki, T.; Kwak, G. Control of Intramolecular Hydrogen Bonding in a Conformation-Switchable Helical-Spring Polymer by Solvent and Temperature. *Angew. Chem., Int. Ed.* **2020**, 59, 1837–1844.
- (70) Giubertoni, G.; Sofronov, O. O.; Bakker, H. J. Effect of intramolecular hydrogen-bond formation on the molecular conformation of amino acids. *Commun. Chem.* **2020**, *3*, No. 84.
- (71) Laurence, C.; Berthelot, M. Observations on the strength of hydrogen bonding. *Perspect. Drug Discovery Des.* **2000**, *18*, 39–60.
- (72) Laurence, C.; Brameld, K. A.; Graton, J.; Le Questel, J.-Y.; Renault, E. The p K BHX database: toward a better understanding of hydrogen-bond basicity for medicinal chemists. *J. Med. Chem.* **2009**, 52, 4073–4086.
- (73) Rumble, J. R. CRC Handbook of Chemistry and Physics; CRC Press, Boca Raton, FL, 2018.
- (74) Biczok, L.; Linschitz, H. Concerted electron and proton movement in quenching of triplet C_{60} and tetracene fluorescence by hydrogen-bonded phenol-base pairs. *J. Phys. Chem. A* **1995**, *99*, 1843–1845.
- (75) Biczók, L.; Gupta, N.; Linschitz, H. Coupled electron-proton transfer in interactions of triplet C₆₀ with hydrogen-bonded phenols: Effects of solvation, deuteration, and redox potentials. *J. Am. Chem. Soc.* **1997**, *119*, 12601–12609.
- (76) Marcus, R. A. Electron transfer reactions in chemistry. Theory and experiment. *Rev. Mod. Phys.* **1993**, *65*, 599.
- (77) Guldi, D. M.; Luo, C.; Prato, M.; Dietel, E.; Hirsch, A. Chargetransfer in a π-stacked fullerene porphyrin dyad: evidence for back electron transfer in the 'Marcus-inverted'region. *Chem. Commun.* **2000**, 373–374.
- (78) Ratera, I.; Sporer, C.; Ruiz-Molina, D.; Ventosa, N.; Baggerman, J.; Brouwer, A. M.; Rovira, C.; Veciana, J. Solvent tuning from normal to inverted marcus region of intramolecular electron transfer in ferrocene-based organic radicals. *J. Am. Chem. Soc.* **2007**, 129, 6117–6129.

- (79) Couture, J.-F.; Hauk, G.; Thompson, M. J.; Blackburn, G. M.; Trievel, R. C. Catalytic roles for carbon-oxygen hydrogen bonding in SET domain lysine methyltransferases. *J. Biol. Chem.* **2006**, *281*, 19280–19287.
- (80) Polander, B. C.; Barry, B. A. A hydrogen-bonding network plays a catalytic role in photosynthetic oxygen evolution. *Proc. Natl. Acad. Sci. U.S.A.* **2012**, *109*, 6112–6117.
- (81) Desai, B. J.; Goto, Y.; Cembran, A.; Fedorov, A. A.; Almo, S. C.; Gao, J.; Suga, H.; Gerlt, J. A. Investigating the role of a backbone to substrate hydrogen bond in OMP decarboxylase using a site-specific amide to ester substitution. *Proc. Natl. Acad. Sci. U.S.A.* **2014**, *111*, 15066–15071.
- (82) Chang, C. J.; Chng, L. L.; Nocera, D. G. Proton-coupled O— O activation on a redox platform bearing a hydrogen-bonding scaffold. *J. Am. Chem. Soc.* **2003**, *125*, 1866—1876.
- (83) Bhunia, S.; Rana, A.; Roy, P.; Martin, D. J.; Pegis, M. L.; Roy, B.; Dey, A. Rational Design of Mononuclear Iron Porphyrins for Facile and Selective 4e–/4H+ O2 Reduction: Activation of O–O Bond by 2nd Sphere Hydrogen Bonding. *J. Am. Chem. Soc.* **2018**, *140*, 9444–9457.
- (84) Chen, J.; Rebek, J. Selectivity in an encapsulated cycloaddition reaction. *Org. Lett.* **2002**, *4*, 327–329.
- (85) Cavarzan, A.; Scarso, A.; Sgarbossa, P.; Strukul, G.; Reek, J. N. Supramolecular control on chemo-and regioselectivity via encapsulation of (NHC)-Au catalyst within a hexameric self-assembled host. *J. Am. Chem. Soc.* **2011**, *133*, 2848–2851.